Experimental and numerical investigation of saltwater intrusion dynamics in flux-controlled groundwater systems

Sun Woo Chang[1] and T. Prabhakar Clement[1]

Received 13 March 2012; revised 25 June 2012; accepted 12 July 2012; published 19 September 2012.

[1] Sea level rise and reduction of groundwater fluxes due to changes in rainfall patterns are the two major climate change–induced hydrological variables that can severely affect saltwater intrusion in coastal aquifers. In this study we use a combination of laboratory experiments and numerical simulations to study the impacts of changes in one of these climate change–induced hydrological variables, groundwater flux, on saltwater intrusion process. We have completed experiments in a laboratory-scale model to study the changes in two types of groundwater fluxes—areal recharge flux and regional flux. The experimental results were modeled using the numerical code SEAWAT. The transient data sets reported in this study are useful benchmarks for testing numerical models that employ flux-type boundary conditions. Also, based on the experimental observations, we hypothesize that when the fluxes are perturbed, it would require relatively less time for a salt wedge to recede from an aquifer when compared to the time required to advance into the aquifer. This rather counterintuitive hypothesis implies that saltwater intrusion and receding processes are asymmetric and the timescales associated with these processes will be different. We use a combination of laboratory and numerical experiments to test this hypothesis and use the resulting data set to explain the reason for the difference in intrusion rates.

Citation: Chang, S. W., and T. P. Clement (2012), Experimental and numerical investigation of saltwater intrusion dynamics in flux-controlled groundwater systems, *Water Resour. Res.*, *48*, W09527, doi:10.1029/2012WR012134.

1. Introduction

[2] Saltwater intrusion is a natural process where seawater would advance into coastal groundwater aquifers due to the density difference between saline and fresh waters, creating a wedge that evolves landward. The horizontal extent of saltwater intrusion could range from a few meters to many kilometers [*Barlow and Reichard*, 2010]. Several natural and anthropogenic processes can enhance the effects of saltwater intrusion. For example, the water supply operations in coastal regions might depend on pumping freshwater from local aquifers, and these pumping activities can exacerbate both vertical and horizontal salt intrusion processes. Droughts induced by climate change effects will result in reduced recharge and this would enhance saltwater intrusion. Several modeling and field studies have provided evidence that climate change could decrease the net freshwater input to groundwater resources [*Feseker*, 2007; *Loáiciga et al.*, 2012; *Masterson and Garabedian*, 2007; *Oude Essink*, 2001; *Oude Essink et al.*, 2010; *Ranjan et al.*, 2006; *Rozell and Wong*, 2010; *Yu*, 2010]. Climate change studies estimate that the global sea level could increase between 18 cm and 59 cm this century [*Intergovernmental Panel on Climate Change* (*IPCC*), 2007]; other worst-case scenario predictions have forecast higher sea level rises up to 180 cm [*Vermeer and Rahmstorf*, 2009], which could result in severe saltwater intrusion.

[3] The number of scientific investigations related to climate change effects have increased rapidly in the last decade [*Green et al.*, 2011]. Most of these investigations are based on the premise that climate change will have severe adverse impacts on almost all natural systems including groundwater systems. As pointed out by *Kundzewicz and Dölle* [2009], flat areas such as deltas and coral islands are expected to be inundated by rising seas leading to reduced freshwater availability. According to an extreme case reported by *Yu* [2010], about a meter sea level rise would inundate and contaminate over 18% of the total land in Bangladesh, threatening to physically displace about 11% of their population.

[4] *Chang et al.* [2011] recently presented some interesting counterintuitive results indicating that sea level rise would have no impact on saltwater intrusion in certain idealized confined systems that ignore marine transgression (inundation of coastline) effects. Their results show that rising seas would lift the entire water table, and this lifting process has the potential to alleviate the overall long-term impacts of saltwater intrusion via a natural self-reversal process. *White and Falkland* [2010] reviewed previously published field data sets and concluded that the freshwater lenses in several atoll islands might not be severely affected by sea level rise up to 1 m, as long as the landmass is not lost due to inundation of the edges of these islands. On the other hand, potential variations in the recharge patterns resulting from changes in the rainfall levels are expected to have much larger impact on the overall water budget of these

[1]Department of Civil Engineering, Auburn University, Auburn, Alabama, USA.

Corresponding author: T. P. Clement, Department of Civil Engineering, Auburn University, Auburn, AL 36849, USA. (clement@auburn.edu)

0043-1397/12/2012WR012134

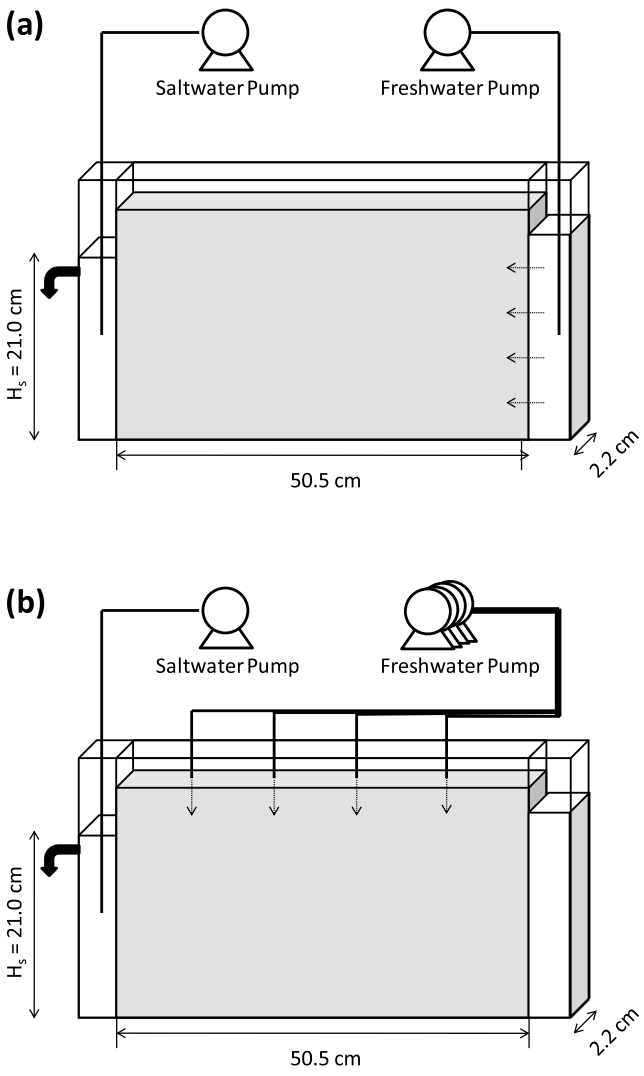

Figure 1. Schematic diagrams of the (a) regional flux and (b) areal recharge flux experiments.

islands. *Rozell and Wong* [2010] used climate change scenarios available in *IPCC* [2007] and found that only a small portion of Shelter Island, located New York, USA, would experience inundation and saltwater intrusion even when the sea level was assumed to increase more than three times higher than those values reported in *IPCC* [2007]. Some of these conflicting results imply that the impacts of climate change on saltwater intrusion should be carefully predicted and managed at a local scale on a case-by-case basis, and the overall impacts would depend on various hydrological factors including spatial and temporal variations in rainfall/recharge patterns.

[5] *Werner and Simmons* [2009] categorized saltwater intrusion problems into two type of systems that depend on the freshwater boundary condition. The first type of system is known as a head-controlled system, where the groundwater level fixed at the inland boundary would transmit various rates of freshwater flow depending on aquifer properties. The second type is a flux-controlled system where the net freshwater flow entering via the aquifer boundary is set to a known flow rate. From a fundamental point of view, even in the head-controlled system the changes in saltwater intrusion patterns would be essentially due to the net decrease or increase in freshwater flow transmitted through the system. Therefore, the amount of freshwater flux moving through the system is an important fundamental parameter that would control saltwater intrusion effects. *Chang et al.* [2011] demonstrated how the impacts of sea level rise on both unconfined and confined systems could be strongly influenced by the changes in freshwater fluxes. *Kuan et al.* [2012] reported that the saltwater wedge and the resulting upper saline plume in unconfined coastal systems will be affected by the changes in the regional freshwater influx induced by the tidal conditions. These studies have demonstrated the importance of understanding the effects of changes in different types of groundwater fluxes on saltwater intrusion mechanisms.

[6] The objective of this research is to conduct experimental studies to investigate the impacts of variations in regional and areal recharge fluxes on saltwater intrusion in unconfined aquifers. In this effort, we have explored two types of flux-controlled systems: one driven by regional flow delivered from the inland freshwater boundary and another driven by a fixed amount of recharge flow distributed from the top. In this work, we refer to these two systems as regional flux and areal recharge flux systems. The results from the experiments were used to develop a better understanding of the influence of flux boundary conditions on the saltwater intrusion process, especially under transient flow conditions.

2. Methods

2.1. Experimental Approach

[7] Figure 1 shows the experimental methods employed in this study. The laboratory setup shown in Figure 1a was used to conduct regional flux aquifer (RFA) experiments, and Figure 1b was used to conduct areal recharge flux aquifer (AFA) experiments. All the experiments were completed in a laboratory tank with dimensions: 50.5 cm $\times$ 28 cm $\times$ 2.2 cm. We used a relatively narrow tank to simulate a two-dimensional system that represents cross-sectional flow in an unconfined aquifer. As shown in Figure 1, the flow tank has three distinct chambers: an inlet chamber, porous media chamber, and an outlet chamber. In the regional flux experiment, the right inlet chamber was used to deliver freshwater flow to the system. The sea level variations were simulated by adjusting the saltwater head at the left outlet chamber. The central porous media chamber was filled with glass beads of diameter 1.1 mm. The beads were packed under saturated conditions to prevent the trapping of air bubbles inside the tank. The average hydraulic conductivity value of the system was estimated to be 1.46 cm/s. Other experimental methods used here were similar to those used in our previous experiments reported in *Goswami and Clement* [2007] and *Abarca and Clement* [2009]. It is important to note that our previous experimental studies (also studies published by others) have used constant head boundary conditions; here we have employed two different types of flux boundary conditions. To simulate the areal recharge flux boundary condition, we used a multihead peristaltic pump that delivered flow at various injection points. The flow was divided equally and was distributed from four outlet tubes. The tubes were placed on the top of a porous media chamber (well above the water table) at distances of 10 cm, 20 cm, 30 cm, and 40 cm away from the inlet chamber. To simulate

Table 1. Summary of Numerical Model Parameters

Property	Symbol	Values
Horizontal length	L	50.5 cm
Saltwater elevation	h_s	21 cm
Hydraulic conductivity	K	1.46 cm/s
Specific yield	S_y	0.1
Specific storage	S_s	0.00001 cm^{-1}
Longitudinal dispersivity	α_L	0.05 cm
Transverse dispersivity	α_T	0.005 cm
Saltwater concentration	Cs	0.0378 g/cm^3
Saltwater density	ρ_s	1.027 g/cm^3
Freshwater density	ρ_f	1.000 g/cm^3

the constant regional flux condition, we used the same multihead pump that injected a constant amount of flow via a single outlet, which was placed into the right chamber. All the saltwater intrusion experiments were recorded using a video camera (Panasonic HDC-HS250) and the pictures were later postprocessed using methods described in *Goswami and Clement* [2007]. A commercial food dye was added at a ratio of 50 ml per 20 L of saltwater to differentiate the saltwater from ambient fresh water. The measured density of the colored saltwater was 1.027 g/cm^3.

2.2. Numerical Modeling Approach

[8] The MODFLOW family variable density flow code SEAWAT [*Guo and Langevin*, 2002] was used to model the experimental data. The fully implicit option and the total variation diminishing (TVD) package were used in all our simulations. This code has been widely tested by solving various benchmark problems including *Simpson and Clement* [2003, 2004] problems. In our model, the origin of an x-z coordinate system was set at the lower left-hand corner of the plane. A uniform finite differences grid of size 0.5 cm (total of 102 cells in the x direction) was used to discretize the horizontal direction. Forty-two confined layers of width 0.5 cm were used to discretize the vertical direction; in addition, a single unconfined layer of width 1 cm was used to represent the top region. The depth of the top layer was selected such that the layer would remain unconfined (i.e., it did not fully drain or overfill) in all our simulations (note that the freshwater head in the tank varied from 21.6 to 22.0 cm, measured from the bottom, in our transient experiments and the saltwater head was set to 21.0 cm). The lower-boundary nodes were set to no-flow conditions. The longitudinal (α_L) and transversal (α_T) dispersivity coefficients were assumed to be 0.05 cm and 0.005 cm, respectively; these are the values previously used by *Abarca and Clement* [2009]. The value of specific storage (S_s) was set to 10^{-6} cm^{-1} for the confined layers and the value of specific yield (S_y) was set to 0.1 for the top unconfined layer. The measured values of freshwater density and the saltwater density were 1.000 and 1.027 g/cm^3, respectively. Using the standard density concentration slope factor of 0.714, the value of salt concentration was estimated to be 0.378 g/cm^3. This concentration value was also verified using data for the amount of salt used to prepare the saltwater solution. The entire flow domain was assumed to be initially filled with saltwater, and a constant rate of freshwater flow was injected at the boundary to simulate the desired initial steady state condition. A summary of the parameters used in the numerical model are given in Table 1.

3. Results

3.1. Regional Flux Experiments

[9] We first completed a regional flux experiment to study the transient changes in saltwater intrusion patterns when the flux was varied at the right boundary. The saltwater level at the left boundary was fixed at 21 cm. Figure 2 shows the digital data collected for both advancing wedge and receding wedge experiments. The time levels required for conducting these experiments were estimated a priori from preliminary numerical simulations. To simulate the initial condition, a constant amount of freshwater (at the rate of 0.832 cm^3/s) was injected into the right chamber and the system was allowed to reach a steady state pattern (designated as SS1 in Figure 2). To start the transient intruding conditions, the flow rate was instantaneously reduced from 0.832 to 0.463 cm^3/s

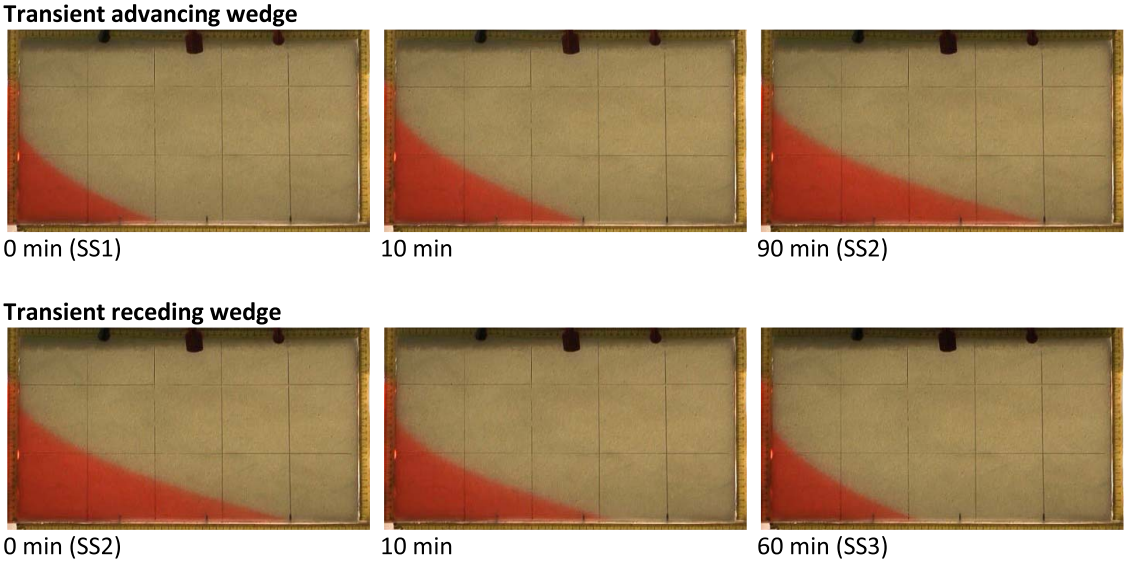

Figure 2. Transient variations in the salt wedge patterns due to changes in the regional flux at the right boundary. (top) Intruding transport conditions when the flow was reduced from 0.833 to 0.467 cm^3/s. (bottom) Receding transport conditions when the flow was increased from 0.467 to 0.833 cm^3/s.

Table 2. Summary of Measured and Modeled Flows

Experiment	Experimentally Measured Flows in the Sand Tank[a] (cm^3/s)	Numerical Flows Used in the Unit-Width Model
RFA test (SS1, SS3)	0.832	0.378 cm^3/s (0.0086 cm^3/s for 42 confined cells, 0.017 cm^3/s for one unconfined cell)
RFA test (SS2)	0.463	0.211 cm^3/s (0.0048 cm^3/s for 42 confined cells, 0.009 cm^3/s for one unconfined cell)
AFA test (SS1, SS3)	1.111	Recharge rate of 0.0100 cm/s
AFA test (SS2)	0.755	Recharge rate of 0.0068 cm/s

[a]With a width of 2.2 cm.

(about 56% of the initial flow). The transient data were recorded for 90 min, after which the system reached the second steady state condition (designated as SS2 in Figure 2). The receding wedge experiment was then initiated by increasing the amount of freshwater flow back to the initial rate of 0.832 cm^3/s. This allowed the wedge to recede back toward the saltwater boundary and the system reached the third steady state condition (designated as SS3 in Figure 2) after 60 min.

[10] Numerical simulations were completed using SEAWAT. The numerical model was assumed to be a unit width aquifer and hence the total flow rate used was set to 0.378 cm^3/s; the real sand tank was, however, 2.2 cm wide and the measured experimental flow rate was 0.832 cm^3/s (Table 2 provides a summary of all these flow values). In the model, the initial total flow of 0.378 cm^3/s was distributed into 0.0086 cm^3/s over 42 confined cells of thickness 0.5 cm; in addition, a 1 cm thick unconfined cell was used and it received a flow rate of 0.017 cm^3/s. To simulate the reduced freshwater flow condition, the flow rates for the confined cells were set to 0.0048 cm^3/s and the top unconfined layer flow was set to 0.009 cm^3/s. The results of the numerical model are compared against the experimental data in Figure 3. In Figure 3, dot-shaped symbols represent experimental observations and the continuous lines represent numerical prediction of 50% concentration contour. Figure 3 shows excellent match between the experimental data and model predictions.

[11] The toe length, X_T, measured at the bottom of the aquifer is a standard metric used for delineating the location of a wedge [*Chang et al.*, 2011; *Watson et al.*, 2010; *Werner and Simmons*, 2009; *Werner et al.*, 2012]. However, in this study, due to some physical irregularities present at the bottom joint of the tank (occurred due to smearing of the excess welding glue outside the tank) prevented us from accurately viewing the wedge at the bottom. This introduced some uncertainties in measuring the length of the saltwater toe X_T (wedge extent at the bottom). To avoid any mismatch due to these uncertainties, we compared the toe length estimated at 0.75 cm above the tank bottom (designated as $X_T@_{0.75}$) against numerical predictions for $X_T@_{0.75}$. Note we selected 0.75 cm since this height conveniently corresponded to the center of a second numerical model layer. Using this upper location allowed us to avoid the observational problem at the bottom of the physical model. Figure 4 compares $X_T@_{0.75}$ predicted by SEAWAT against the values evaluated from the transient experimental data for both advancing and receding experiments. Figure 4 shows that the

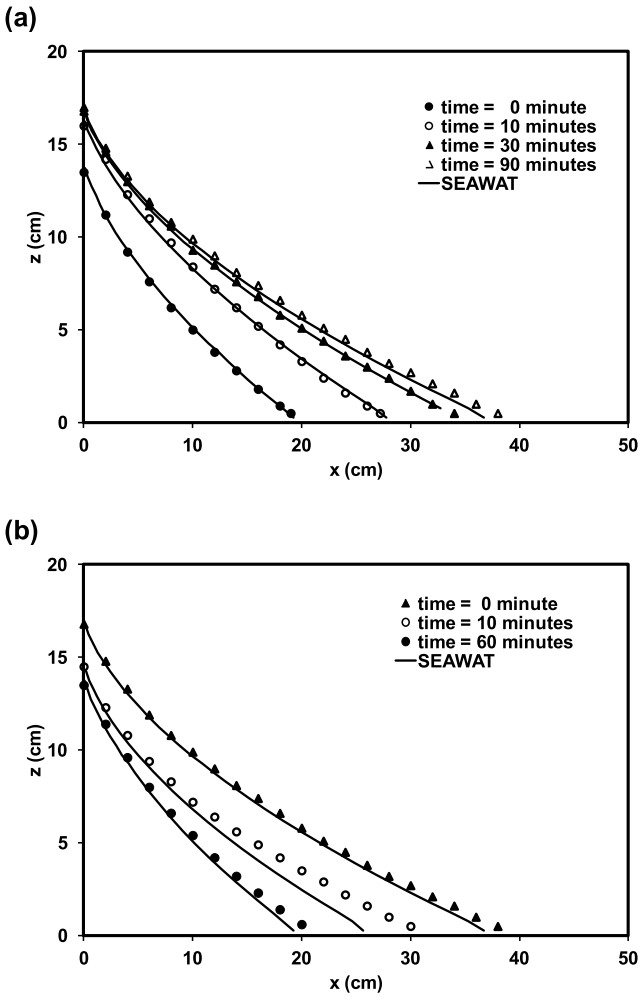

Figure 3. Comparison of experimental data with model-predicted transient salt wedges for the regional flux system: (a) advancing wedge experiment and (b) receding wedge experiment.

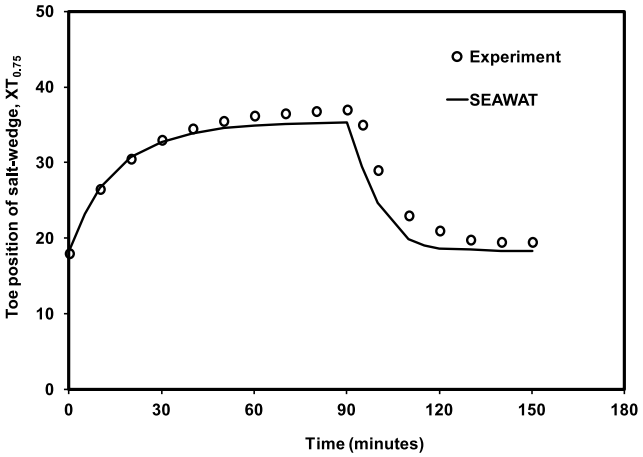

Figure 4. Comparison of experimental and model-simulated toe positions estimated at 0.75 cm above tank bottom in the regional flux experiment.

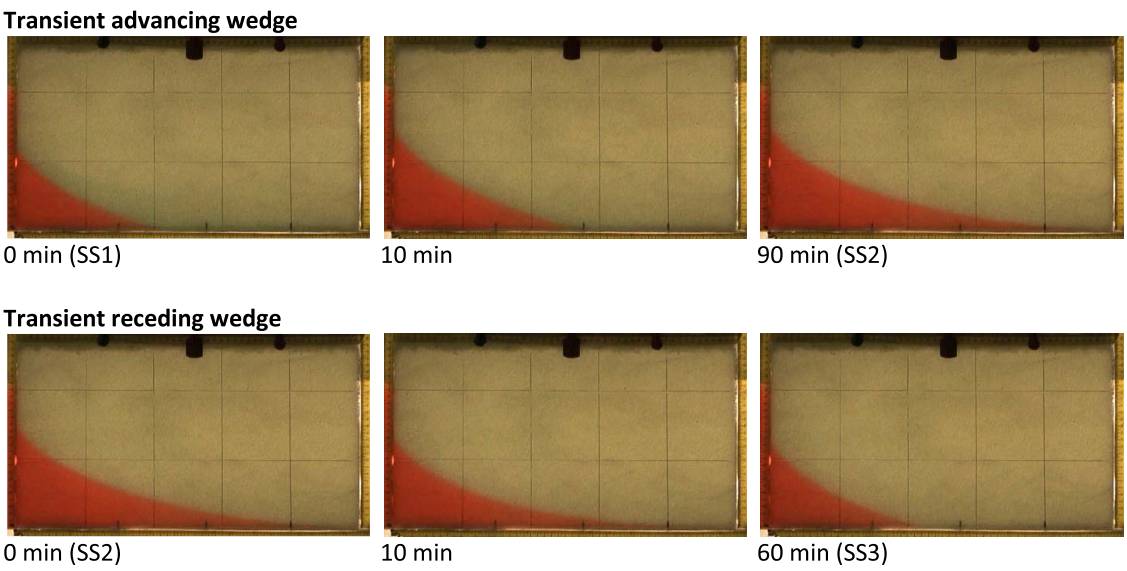

Figure 5. Transient variations in the salt wedge patterns due to changes in the areal flux values. (top) Intruding transport conditions when the flow was reduced from 1.111 to 0.755 cm^3/s. (bottom) Receding transport conditions when the flow is increased from 0.755 to 1.111 cm^3/s.

numerical model was able to predict the saltwater toe lengths of both intruding and receding wedges.

3.2. Areal Recharge Flux Experiments

[12] The areal recharge flux experiments were completed to study the extent of saltwater intrusion when the recharge flux varied at the top of the model. In all these experiments, the saltwater level was fixed at 21 cm at the left boundary. Figure 5 shows the digital data for the advancing and receding wedge experiments. The experiment was designed such that the length of wedge in the current (areal flow) system was almost similar to the wedge in the previous (regional flow) system, providing similar-looking wedge profiles. The time levels and flow rates required for the experiment were designed using preliminary test simulations. Note that the rate of freshwater flow used in the areal recharge test was larger than the flow used in the regional flux test; this increase was required to create a wedge profile similar to the previous test. If we would have used similar flow rates, the wedge in the areal recharge experiment would have intruded much less into the aquifer.

[13] To begin the areal flux experiment, a constant total freshwater flow rate of 1.111 cm^3/s was injected at the top of the tank and the system was allowed to reach a steady state pattern (designated as SS1 in Figure 5). To initiate transient conditions, flow rate was instantaneously reduced to 0.755 cm^3/s (about 68% of the initial flow rate), which then allowed the wedge to advance to the right, toward the flux boundary, by ~20 cm. The transient data were recorded for 90 min, after which the system reached the second steady state condition (designated as SS2 in Figure 5). Then, the receding wedge experiment was initiated by increasing the amount of freshwater flow back to the initial rate of 0.505 cm^3/s. The wedge started to recede backward toward the saltwater boundary and reached the third steady state (designated as SS3 in Figure 5) and the transport data were recorded for 60 min.

[14] Numerical simulations were completed using SEAWAT. In the numerical model, the initial areal recharge rate of 0.010 cm/s (same as, 1.111 cm^3/s/50.5 cm × 2.2 cm) was set using the recharge package. To simulate the instantaneous reduction in the freshwater recharge, the rate was reduced to 0.0068 cm/s. The numerical predictions are compared against the experimental data in Figure 6. Figure 6 shows good match between the experimental data and numerical predictions. Similar to previous experiments, in order to avoid the observational errors associated with our tank bottom, we compared the experimental values of X_T observed at 0.75 cm (above the tank bottom) against the corresponding X_T values computed by the numerical model. The results shown in Figure 7 compare the transient variations in toe length ($X_T@_{0.75}$) predicted by SEAWAT against data for both intruding and receding areal recharge flux experiments. The results show that the model was able to predict the experimental data well.

3.3. Analysis of Timescales Associated With Intruding and Receding Salt Wedges

[15] The transient data for the regional flux experiment, presented in Figure 4, show that the intruding wedge requires more time to reach steady state when compared to the receding wedge. This trend is also observed in the recharge flux experiment shown in Figure 7. Previously published experimental data presented by *Goswami and Clement* [2007] for a constant head system also indicated a similar trend. This is an interesting and rather counterintuitive result which implies that it will take relatively less time to remediate (or reverse) a saltwater intrusion system when compared to the time taken to contaminate (or advance the wedge into) the system. This is a subtle yet an important result that can play a significant role in managing the water quality of coastal aquifers. However, so far no one has either quantified or analyzed the disparities in the timescales associated with saltwater intrusion and recession processes.

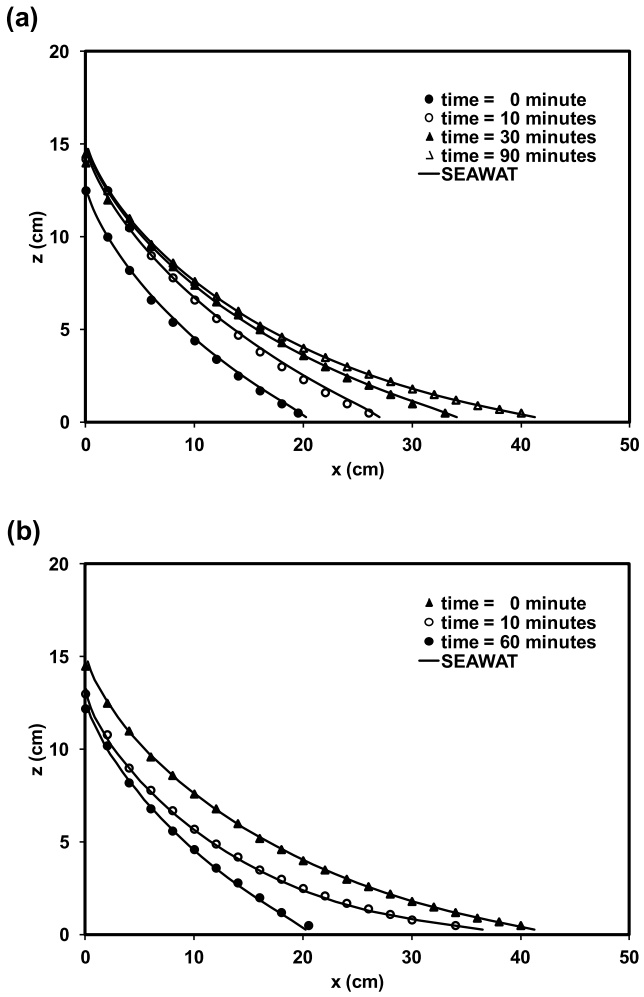

Figure 6. Comparison of experimental data with model-predicted transient salt wedges for the areal flux system: (a) advancing wedge experiment and (b) receding wedge experiment.

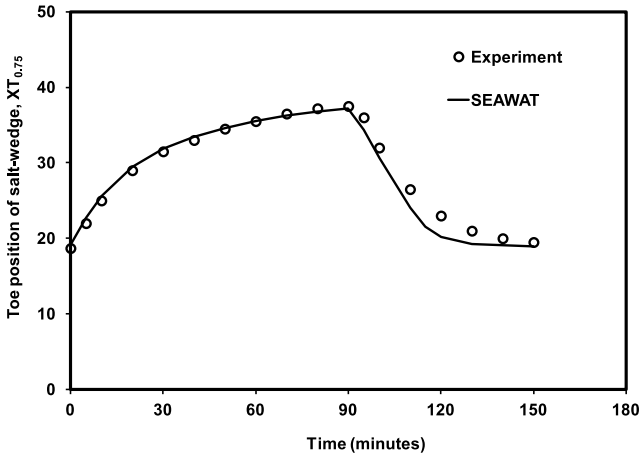

Figure 7. Comparison of experimental and model-simulated toe positions estimated at 0.75 cm above tank bottom in the areal flux experiment.

[16] In order to quantify the difference between intruding and receding wedge migration rates, we first define a term $\Delta X_T(t)$, which is the distance that remains to be traversed by a migrating saltwater wedge toe to reach its final steady state condition (note, we will be using numerical data in this analysis and report the estimates of X_T at the bottom of the aquifer). Using this definition, for an intruding wedge $\Delta X_T(t) = ABS[X_T(t) - X_{T\ for\ SS2}]$, and for a receding wedge $\Delta X_T(t) = ABS[X_T(t) - X_{T\ for\ SS3}]$. Note in our experiments the final steady state SS3 is identical to the initial steady state SS1. For the regional flux test, the values of $X_{T\ for\ SS1}$ (or $X_{T\ for\ SS3}$) and $X_{T\ for\ SS2}$ were estimated using SEAWAT as 19.3 and 36.8 cm, respectively. The computed values of $\Delta X_T(t)$ for both intruding and receding wedges are presented in Figure 8a. Figure 8a clearly shows that the receding wedge moves considerably faster than the intruding wedge. The function $\Delta X_T(t)$ resembles a first-order decay process, and hence one could fit an exponential decay curve of the form $\Delta X_T(t) = \Delta X_{T0} \exp(-t/\tau)$ to these data; where, the parameter ΔX_{T0} is the maximum distance traversed by a moving wedge, and τ is a characteristic time constant. It should be noted that this approximate fitting analysis was completed simply to estimate an "effective characteristic time" for this

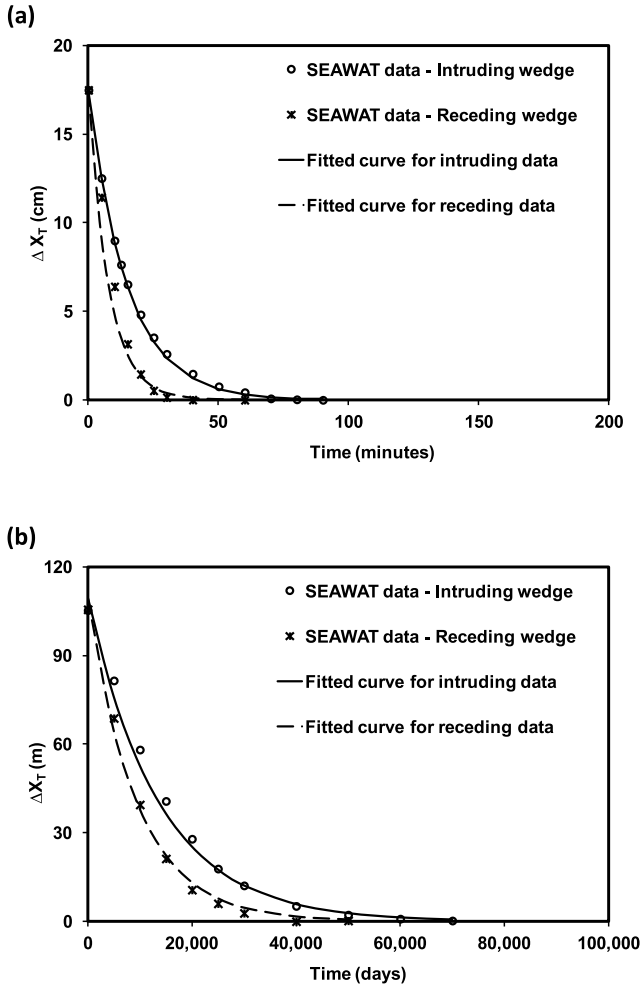

Figure 8. Comparison of toe migration rates of intruding and receding wedges for the (a) laboratory-scale regional flux problem and (b) field-scale problem reported in *Chang et al.* [2011].

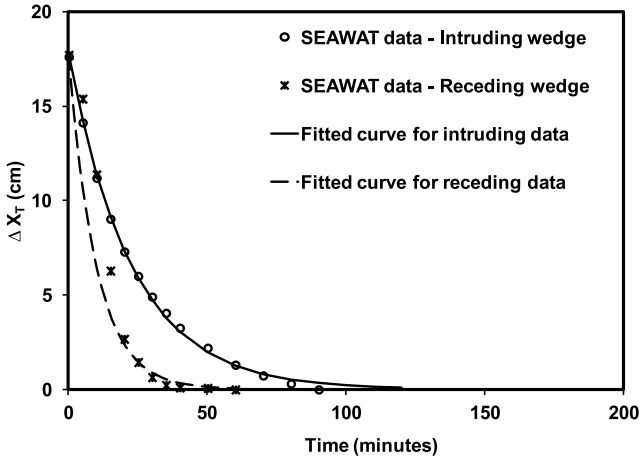

Figure 9. Comparison of toe migration rates of intruding and receding wedges for the laboratory-scale areal recharge problem.

rather complex transient problem. For the regional flux case, the value of ΔX_{T0} was calculated as 17.5 cm [ABS ($X_{T\ for\ SS1} - X_{T\ for\ SS2}$)], and the fitted values of τ for intruding and receding wedges were estimated to be 15.0 and 7.9 min, respectively. The time constant τ is an integrated measure of the characteristic time associated with the underlying transport processes. The value of τ computed for the intruding system is larger than the value computed for the receding system, indicating that the intrusion process is inherently slower than the recession process. Based on this result one could hypothesize that it will take relatively less time for a salt wedge to recede from an aquifer when compared to the time taken for the wedge to intrude into an aquifer. To test the validity of this hypothesis at a larger scale, we completed a simulation study for a large-scale problem reported in *Chang et al.* [2011]. The problem considered a two-dimensional unconfined aquifer system which is 1000 m long and 31 m thick with unit width. The sea level was set at 30 m along the left boundary. A regional flow of 0.186 m^3/d was injected at the right boundary. The initial steady state (SS1) location of the salt wedge toe, $X_{T\ for\ SS1}$, was 380 m away from the coastal boundary. To initiate transient intrusion conditions, the boundary flux was instantaneously reduced to 0.140 m^3/d (about 75% of the initial flux) which allowed the wedge to advance toward the landward direction. It took ~60,000 days for the system to reach the second steady state (SS2), and value of $X_{T\ for\ SS2}$ was 485 m. The receding wedge experiment was then initiated by restoring the freshwater flux back to the initial flow rate of 0.186 m^3/d. The wedge started to recede back and reached the third steady state (SS3) after about 40,000 days. In Figure 8b, we provide the $\Delta X_T(t)$ profiles for both intruding and receding simulations. The value of ΔX_{T0} estimated for the system was 105 m (485 m–380 m), and the fitted values of the time constants (τ) for the intruding and receding wedges were 13,600 and 9400 days, respectively.

[17] To compare the differences in intruding and receding transport timescales under areal recharge flux boundary conditions, we completed another set of simulations and compiled $\Delta X_T(t)$ data for the areal experimental problem. The initial rate of recharge used in the simulation was 0.0102 cm/sec and the corresponding value of $X_{T\ for\ SS1}$ was 19.7 cm. The recharge was then reduced to 0.0071 cm/sec and the corresponding value of $X_{T\ for\ SS2}$ was 37.3 cm. Note that the recharge rates for this theoretical problem were selected to obtain X_T values (and also the corresponding ΔX_{T0} value) almost identical to the regional flux problem. Figure 9 shows the SEAWAT simulated $\Delta X_T(t)$ data and the fitted exponential profiles. Similar to the previous problem, the intruding wedge moved slower than the receding wedge even under areal recharge flux conditions. The simulated data for the receding wedge however, did not show a smooth exponential trend. We evaluated the model parameters for the best fit exponential functions and used them to estimate the values of the time constants for the intrusion and receding wedges as 22.7 and 10.1 min, respectively. These results once again confirm that the transport time required for the intruding wedge is more than the time required for the receding wedge.

[18] To understand the fundamental reason for the difference in the transport timescales, we analyzed the underlying velocity distribution (or flow field) near the intruding and receding wedges. Figure 10 shows the model-predicted vector field for the regional flux system at the two steady state conditions SS1 and SS2. The length of each velocity vector presented in Figure 10 is directly proportional to the magnitude of the velocity. Figure 10 also shows the 50% concentration contour to delineate the wedge location. Several interesting observations can be made from these steady state data. First, the vector field shows that the velocities in the freshwater region above the wedge are much higher than the velocities in the saltwater region (velocity vectors of salt water are small and we will use log scale to better visualize these vectors in Figure 12). It can be observed that the freshwater flow from inland boundary converges into the narrow zone above the salt wedge and discharges within a high-velocity region as it approaches the seaside boundary. On the contrary, saltwater flow velocities below the wedge are small within this relatively stagnant region. Upon closer review one could observe a convection cell circulating saltwater beneath the wedge. Also, there is a stagnation point

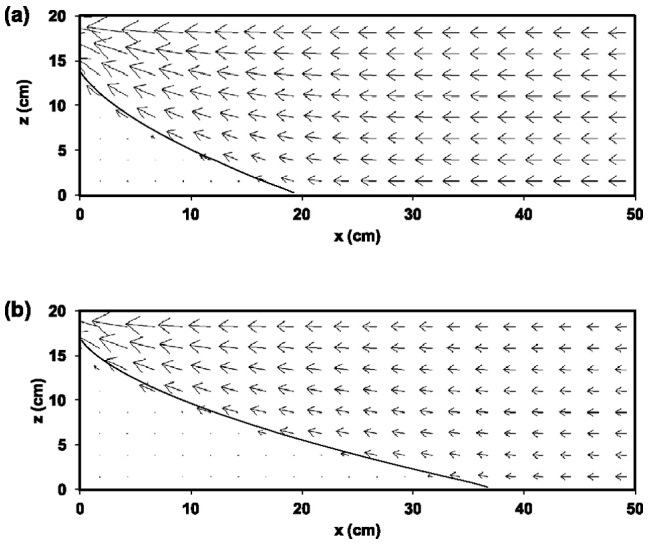

Figure 10. Simulated steady state velocity fields for the regional flux experiment (a) SS1 and (b) SS2.

(with opposing flow vectors) present close to the toe of the wedge at the bottom of the aquifer.

[19] To better understand the transport dynamics under transient conditions, we plotted the velocity fields for both intruding and receding wedge after two minutes of transport (i.e., two minutes after the steady state condition was perturbed). These data are shown in Figure 11. In order to better visualize the low-velocity vectors present beneath the salt wedge, we transformed the velocity vector field into log scale and Figure 12 shows the vector field computed at various times. The first picture, Figure 12a, simply presents the steady state (SS1) data shown in Figure 10a in logarithmic scale. One could now clearly see the circulation cell and the stagnation point (present at around 20 cm) in this log-transformed velocity vector plot. Note, under the wedge, saltwater continuously enters the aquifer from the bottom and exists near the interface, forming a convection cell.

[20] Figures 11a and 12b show the velocity fields of the transient intruding salt wedge (2 min of transport after SS1). Figures 11a and 12b show that the saltwater transport process distorts the convection cell when wedge is migrating into the aquifer. All the vectors below the wedge are now pointing toward the landward direction. Within 2 min, the stagnation point has been pushed into the system by about 26 cm. The relative magnitude of saltwater velocities are small (see Figure 11a), and the saltwater flow vectors are diametrically opposite to the freshwater flow vectors forming a stagnation region where the velocities reverse; also, a distinct stagnation point continue to persist at the aquifer bottom (see Figure 12b). In the intruding system, the saltwater wedge advances slowly against an opposing fresh water flow field. Once the steady state condition is reached (Figure 12c) the convection cell was restored.

[21] Figures 11b and 12d show the velocity fields of the receding wedge in regular scale and log scale, respectively, after 2 min of transport from SS2. A direct comparison of intruding and receding flow fields, presented in Figures 11a and 11b, respectively, shows that the receding system is characterized by much higher velocities since the net freshwater flux transmitted through the system is higher in this case. Log-scaled velocities shown in Figure 12d clearly show that once the fresh water flux was increased, to initiate the receding condition, the direction of saltwater water flow was reversed toward seaward direction. This flow reversal, however, is only a transient phenomenon caused by the sharp increase in the freshwater flux and the associated transient changes in groundwater head values. Unlike the intruding system, which supports opposing flow fields, here the flow field is unidirectional with all the vectors pointing toward the saltwater boundary and hence there is no stagnation point in this system. Since the flow field is well aligned, the transport processes associated with a receding wedge can flush the saltwater rapidly out of the system thus facilitating faster wedge movement.

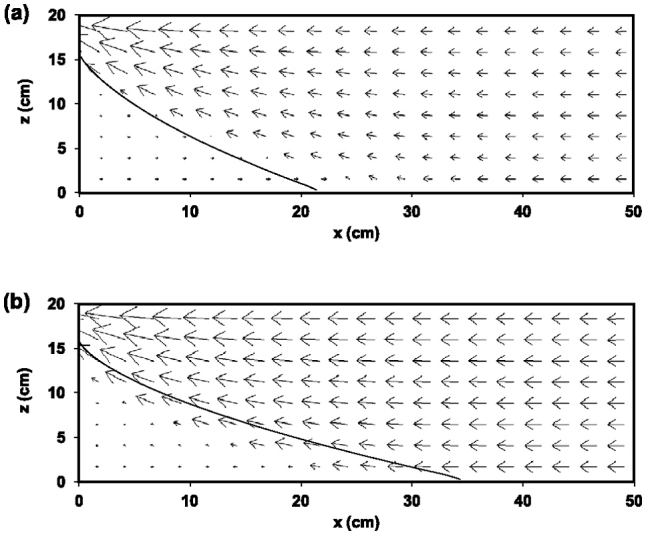

Figure 11. Simulated transient velocity fields for the regional flux experiment (a) 2 min after SS1 and (b) 2 min after SS2.

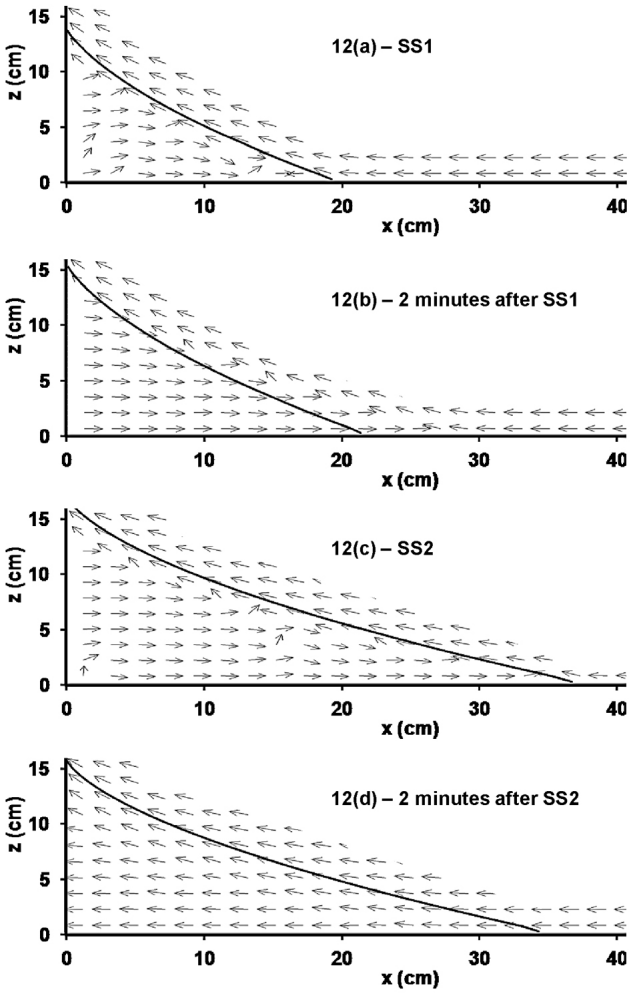

Figure 12. Visualization of the velocity fields near the salt wedge plotted in log scale at (a) SS1, (b) 2 min after SS1, (c) SS2, and (d) 2 min after SS2.

4. Conclusions

[22] Sea level rise and reduction of recharge due to changes in rainfall patterns (and the associated changes in groundwater fluxes) are the two major climate change–induced hydrological processes that can affect saltwater intrusion processes in coastal aquifers. The objective of this

research was to conduct laboratory-scale experiments to investigate the impacts of variations in regional and areal recharge fluxes on saltwater intrusion in unconfined aquifers. We have successfully completed laboratory experiments to study two types of flux-controlled saltwater intrusion problems: one controlled by the regional flow delivered from the inland freshwater boundary, and the other controlled by the recharge flow delivered from the top boundary. The results of the experiments are useful for developing a better understanding for the influence of changes in boundary fluxes on transient saltwater intrusion processes. The experimental data presented in this study are also useful benchmarks for testing the validity of density-coupled flow and transport models involving flux-type boundary conditions.

[23] Based on our experimental data, we hypothesized that the timescales associated with an intruding wedge would be higher than a receding wedge. This hypothesis was tested using numerical simulations completed for problems involving two different scales (1 m and 1000 m scales). Our analysis also shows that the intruding system supports two opposing flow fields with a distinct stagnation point at the bottom of the aquifer, and a diffused stagnation zone along the wedge where the flow velocities reverse direction. On the other hand, the receding system supports a unidirectional flow field with all the velocity vectors pointing toward the saltwater boundary. Due to the presence of opposing flow fields the time taken for saltwater to intrude into an aquifer will be relatively high when compared to the time taken for the saltwater to recede out of an aquifer (which has a well-aligned unidirectional flow field). Currently, transient wedge migration data sets are not available in the published literature to demonstrate these trends for a field problem. However, *Michael et al.*'s [2005] field study, which provided modeling calculations for characterizing seasonal oscillations in water exchange between the aquifer and ocean at Waquoit Bay, Massachusetts, appears to show similar trends. Their simulations indicate that when the seasonal recharge was increased the amount of saltwater flux transmitted into the system decreased sharply, indicating a rapidly receding salt wedge. On the other hand, when the recharge was decreased the amount of saltwater flux increased rather gently, indicating a slowly advancing wedge.

[24] Overall, the insights gained from this study are not only useful for managing saltwater wedges, but are also useful for understanding solute transport processes occurring within a transient saltwater wedge. These transport processes could be coupled to multispecies reactive transport formulations [e.g., *Clement et al.*, 1998; *Sun and Clement*, 1999] to predict the exchange of nutrients and other contaminants between terrestrial and marine waters. In summary, this study has the following two major contributions: (1) the experimental efforts report transient saltwater intrusion data for systems involving two types of flux boundary conditions, and these data can be used for benchmarking numerical formulations; and (2) the experimental observations together with the numerical results point out the difference in timescales between intruding and receding saltwater wedges, and offer a mechanistic explanation for the difference.

[25] **Acknowledgments.** Authors wish to thank Matthew Simpson and Rohit Goswami for their time and support. This work was supported in part by the Samuel Ginn College of Engineering dean fellowship awarded to Sun Woo Chang at Auburn University.

References

Abarca, E., and T. P. Clement (2009), A novel approach for characterizing the mixing zone of a saltwater wedge, *Geophys. Res. Lett.*, *36*, L06402, doi:10.1029/2008GL036995.

Barlow, P. M., and E. G. Reichard (2010), Saltwater intrusion in coastal regions of North America, *Hydrogeol. J.*, *18*, 247–260, doi:10.1007/s10040-009-0514-3.

Chang, S. W., T. P. Clement, M. J. Simpson, and K.-K. Lee (2011), Does sea-level rise have an impact on saltwater intrusion?, *Adv. Water Resour.*, *34*, 1283–1291, doi:10.1016/j.advwatres.2011.06.006.

Clement, T. P., Y. Sun, B. S. Hooker, and J. N. Petersen (1998), Modeling multispecies reactive transport in ground water, *Ground Water Monit. Rem.*, *18*, 79–92, doi:10.1111/j.1745-6592.1998.tb00618.x.

Feseker, T. (2007), Numerical studies on saltwater intrusion in a coastal aquifer in northwestern Germany, *Hydrogeol. J.*, *15*, 267–279, doi:10.1007/s10040-006-0151-z.

Goswami, R. R., and T. P. Clement (2007), Laboratory-scale investigation of saltwater intrusion dynamics, *Water Resour. Res.*, *43*, W04418, doi:10.1029/2006WR005151.

Green, T. R., M. Taniguchi, H. Kooi, J. J. Gurdak, D. M. Allen, K. M. Hiscock, H. Treidel, and A. Aureli (2011), Beneath the surface of global change: Impacts of climate change on groundwater, *J. Hydrol.*, *405*, 532–560, doi:10.1016/j.jhydrol.2011.05.002.

Guo, W., and C. D. Langevin (2002), *User's Guide to SEWAT: A Computer Program for Simulation of Three-Dimensional Variable-Density Ground-Water Flow*, U.S. Geol. Surv., Reston, Va.

Intergovernmental Panel on Climate Change (IPCC) (2007), *Climate Change 2007: Impacts, Adaptation and Vulnerability. Contribution of Working Group II to the Fourth Assessment Report of the Intergovernmental Panel on Climate Change*, edited by M. L. Parry et al., Cambridge Univ. Press, Cambridge, UK.

Kuan, W. K., G. Jin, P. Xin, C. Robinson, B. Gibbes, and L. Li (2012), Tidal influence on seawater intrusion in unconfined coastal aquifers, *Water Resour. Res.*, *48*, W02502, doi:10.1029/2011WR010678.

Kundzewicz, Z. W., and P. Dölle (2009), Will groundwater ease freshwater stress under climate change?, *Hydrol. Sci. J.*, *54*, 665–675, doi:10.1623/hysj.54.4.665.

Loáiciga, H. A., T. J. Pingel, and E. S. Garcia (2012), Sea water intrusion by sea-level rise: Scenarios for the 21st century, *Ground Water*, *50*, 37–47, doi:10.1111/j.1745-6584.2011.00800.x.

Masterson, J. P., and S. P. Garabedian (2007), Effects of sea-level rise on ground water flow in a coastal aquifer system, *Ground Water*, *45*, 209–217, doi:10.1111/j.1745-6584.2006.00279.x.

Michael, H. A., A. E. Mulligan, and C. F. Harvey (2005), Seasonal oscillations in water exchange between aquifers and the coastal ocean, *Nature*, *436*, 1145–1148, doi:10.1038/nature03935.

Oude Essink, G. H. P. (2001), Salt water intrusion in a three-dimensional groundwater system in the Netherlands: A numerical study, *Transp. Porous Media*, *43*, 137–158, doi:10.1023/A:1010625913251.

Oude Essink, G. H. P., E. S. van Baaren, and P. G. B. de Louw (2010), Effects of climate change on coastal groundwater systems: A modeling study in the Netherlands, *Water Resour. Res.*, *46*, W00F04, doi:10.1029/2009WR008719.

Ranjan, P., S. Kazama, and M. Sawamoto (2006), Effects of climate change on coastal fresh groundwater resources, *Global Environ. Change*, *16*, 388–399, doi:10.1016/j.gloenvcha.2006.03.006.

Rozell, D. J., and T.-F. Wong (2010), Effects of climate change on groundwater resources at Shelter Island, New York State, USA, *Hydrogeol. J.*, *18*, 1657–1665, doi:10.1007/s10040-010-0615-z.

Simpson, M. J., and T. P. Clement (2003), Theoretical analysis of the worthiness of Henry and Elder problems as benchmarks of density-dependent groundwater flow models, *Adv. Water Resour.*, *26*, 17–31, doi:10.1016/S0309-1708(02)00085-4.

Simpson, M. J., and T. P. Clement (2004), Improving the worthiness of the Henry problem as a benchmark for density-dependent groundwater flow models, *Water Resour. Res.*, *40*, W01504, doi:10.1029/2003WR002199.

Sun, Y., and T. P. Clement (1999), A decomposition method for solving coupled multi-species reactive transport problems, *Transp. Porous Media*, *37*, 327–346, doi:10.1023/A:1006507514019.

Vermeer, M., and S. Rahmstorf (2009), Global sea level linked to global temperature, *Proc. Natl. Acad. Sci. U. S. A.*, *106*, 21,527–21,532, doi:10.1073/pnas.0907765106.

Watson, T. A., A. D. Werner, and C. T. Simmons (2010), Transience of seawater intrusion in response to sea level rise, *Water Resour. Res.*, *46*, W12533, doi:10.1029/2010WR009564.

Werner, A. D., and C. T. Simmons (2009), Impact of sea-level rise on sea water intrusion in coastal aquifers, *Ground Water*, *47*, 197–204, doi:10.1111/j.1745-6584.2008.00535.x.

Werner, A. D., J. D. Ward, L. K. Morgan, C. T. Simmons, N. I. Robinson, and M. D. Teubner (2012), Vulnerability indicators of sea water intrusion, *Ground Water*, *50*, 48–58, doi:10.1111/j.1745-6584.2011.00817.x.

White, I., and T. Falkland (2010), Management of freshwater lenses on small Pacific islands, *Hydrogeol. J.*, *18*, 227–246, doi:10.1007/s10040-009-0525-0.

Yu, W. (2010), *Implications of Climate Change for Fresh Groundwater Resources in Coastal Aquifers in Bangladesh*, World Bank, Washington, D. C.